PIV Measurements of the Vortical Wake Behind Tilt-rotor Blades

Charlie Barla [1], Daniel Favier[1], Christophe Rondot[1], Christian Maresca[1]
Markus Raffel[2], Hughes Richard[2], Johannes Bosbach[2], Harnes Henning[2]

1: Department LABM, Aerodynamics and Biomechanics of Motion Laboratory,
CNRS and University of Mediterranee, CP 918, F-13288 Marseille Cedex 09, France, daniel.favier@univmed.fr
2: DLR, Institute of Aerodynamics and Flow Technology,
Bunsenstrasse 10, D-37073 Göttingen, Germany, markus.raffel@dlr.de

Abstract This paper concerns a collaborative research work between DLR of Göttingen and LABM of Marseille which aims to create a new experimental data base characterizing the tilt-rotor wake and the associated vortex structures. This study will provide detailed flow data on the aerodynamic interactions causes which occur on a tilt-rotor aircraft including a rotor, a nacelle, a fixed wing and an end plate simulating the fuselage. Experiments have been performed in the LABM S1L wind-tunnel at 3 different flight configurations which correspond to hover, conversion and cruise flights. The stereoscopic PIV system generates an illuminating laser sheet in a Z-plane normal to the uniform free stream velocity U_8. PIV measurements have been performed at different Z-planes distributed at different distance downstream the rotor (in the wake region between the rotor and the wing and above the fixed wing) in both the conversion and cruise flight configurations and for different parametric conditions of the rotor shaft angle (β), the blade rotational frequency (f), the upstream velocity (U_8), the advancing parameter ($\mu=U_8/2\pi fR$) and the collective pitch angle value (θ). For these different parametric conditions the tip vortex path and the associated 3C velocity field shed from the blade have been determined in the early stages of the tip vortex shedding corresponding to 3 azimuth positions (ψ=1°, 2°, 5°) and in a fixed downstream plane located at Z/R=0. The XY-plots of the velocity vector clearly show the flow perturbation generated by the blade passage and the vortex development and propagation from the tip of the emitting blade. Moreover, from such PIV measurements performed at different downstream distances from the rotor and at different blade azimuth positions the tip vortex paths have been reconstructed both in the wake region between the rotor and the wing and above the wing surface. The wake data provide a better understanding on both the vortex dynamics and the behaviour of vortical structures interacting with the wing on a tilt-rotor configuration.

1. Introduction

In recent years, significant progresses have been done in the aerodynamic performance prediction of tilt-rotor blades operating at different flight conditions. However detailed experimental data bases are still needed to improve and validate CFD methods. Indeed, flow features around tilt-rotor blades are subject to aerodynamic interactions between the rotor, the nacelle and the fixed wing directly placed in the wake and are shown to be strongly dependent on the different flight conditions. Felker and Light (1988) have studied such interactions which are exhibiting a download phenomenon on the wing in hovering flight. Later, Matos et al. (1999) have also quantified this download behaviour for different flap angles values on the wing. Young et al. (2002) have shown that the wing download is generated at the root of the wing and extends along the span. Moreover, by means of pressure coefficients integrations, they have shown that the wing download (DL/C_T) was nearly equal to 0.105 which is a value very close to those of Felker et al. (1987) and McVeigh et al. (1990). It has also been demonstrated in previous works that the airframe contribution to total download is very important in the hovering flight configuration. This is in accordance with the value of about 40% of total download measured by Wood and Peryea (1986). More recent studies (like Johnson, 2000) have quantified the aerodynamic interactions thanks to improvements in aircraft design. But they also reveal that a better understanding of the rotor wake evolution seems to be required in order to reduce aerodynamic interaction effects for one tilt-rotor aircraft geometry. In

addition to this, it should be considered that tilt-rotor blades aerodynamics is generally fundamentally different from helicopter ones. In such a way, tilt-rotor wake modeling should be strongly improved by means of suited experimental data providing a better understanding of vortex dynamics as recently studied by Richard (2005) for helicopters rotor in a forward flight configuration.

For hovering flight conditions, Meakin (1995) developed a Navier-Stokes code around moving body to model the flow on a V-22 tilt-rotor in the presence of half a span wing below it. However the Figure of Merit (FM) was quite under-predicted when compared to experimental data which have been obtained by Felker et al. (1987). One of the most efficient modeling improvement was made by Johnson (1992-1997) who developed the numerical tool called CAMRAD II. This last one is based on the second order of the lifting lines theory and using a vortex wake model to calculate induced velocities. However, global and local aerodynamic performances are shown to be more and more dependent on the accuracy of the wake evolution and explain the fact that a lot of research works have been recently done for accurately modeling the rotor wake distortion due to the wing presence.

For cruise flight conditions, Johnson (2002) has compared the influence of two different wake models which take into account the delay of the boundary layer separation due to centrifugal effects as observed by Barla et al. (in press) : a simple rolled-up wake model (RUWM) where the formation of the tip vortex is the same as for a helicopter blade and a multiple trailer wake model (MTWM), where the viscous effects are not taken into account but coupled with a wake model in order to better estimate the vortex path. MTWM provides better correlations with experiments than RUWM, and predict a more accurate field vorticity data for low thrust coefficients. The results concerning lower thrust coefficients have also been studied by Yamauchi et al. (1999) by means of 2C PIV measurements. This experiment constitutes one of the first wake vortices measurements in airplane mode on a tilt-rotor configuration. Results specially show that tangential velocity component in the vortex core was proportional to the vortex size.

It is worth noting that there exists a relatively poor literature concerning the study of the transition and/or conversion flight configurations. Indeed, almost works attempt to develop and validate numerical models in order to gain insight in simple flight configurations. However it will be challenge from now to investigate such flight configurations which involve more complex parametric conditions and flow features.

An improved understanding of vortex dynamics in the vicinity of the blades thus appear to be a very important key to improve and validate actual numerical codes. Moreover, the path and evolution of the vortices in the near wake rotor, just before the interaction process with the wing, will also provide the requested flow conditions associated with the modeling of aerodynamic interaction effects on the fixed wing for different flight conditions. Tip vortex paths and vortex dynamics have been thus determined using 3C PIV measurements in the present study.

2. Experimental Method and Procedure

2.1 Tilt-rotor Experimental Set-up

Experiments have been performed on a scaled tilt-rotor model set-up in the LABM S1L wind-tunnel at 3 different flight configurations which correspond to hover, conversion and cruise flights as shown in figure 1.

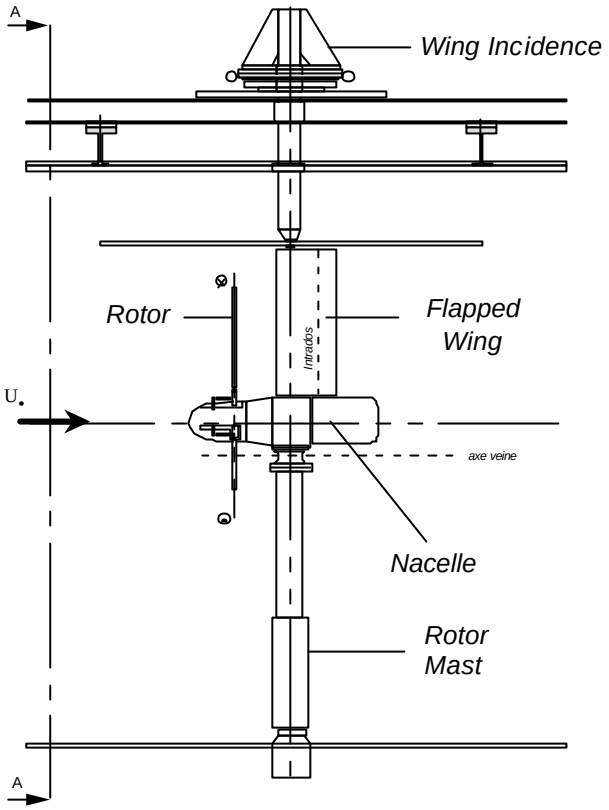

Fig. 1. Schedule of Tilt-rotor configuration

The rotor (diameter D=0.140m, radius R=0.7m and a hub diameter D_0=0.27m) is fully articulated and equipped with a nacelle and 3 blades having non linear twist and chord laws and different airfoil profiles along the blade span as shown in Table 1.

Table 1: Blade geometry definition

r/R	**Radius r (m)**	**Twist angle** q **(deg)**	**Chord C (m)**	**Profile**
0,278	0,195	18,00	0,1025	*OH120*
0,300	0,210	17,00	0,1025	*OH120*
0,400	0,280	11,20	0,1025	OH120
0,480	0,336	7,20	0,1025	
0,500	0,350	6,20	0,0990	*OA312*
0,650	0,455	1,55	0,0726	*OA312*
0,700	0,490	0	0,0717	*OA312*
0,800	0,560	-3,10	0,0700	
0,900	0,630	-5,70	0,0683	*OA309*
1,000	0,700	-7,50	0,0666	*OA309*

The rotor is mounted in the V1 wind-tunnel test section (3m in diameter, 6m in length, maximum velocity 100 ms^{-1}) by means of a vertical cylindrical mast which can be rotated of a shaft angle β, with an accuracy of 0.025deg on the direction of the upstream velocity, in order to simulate the hovering flight (β=90° in figure 2a), the conversion (β=45° in figure 2b) and the cruise (β=0° in figure 2c).

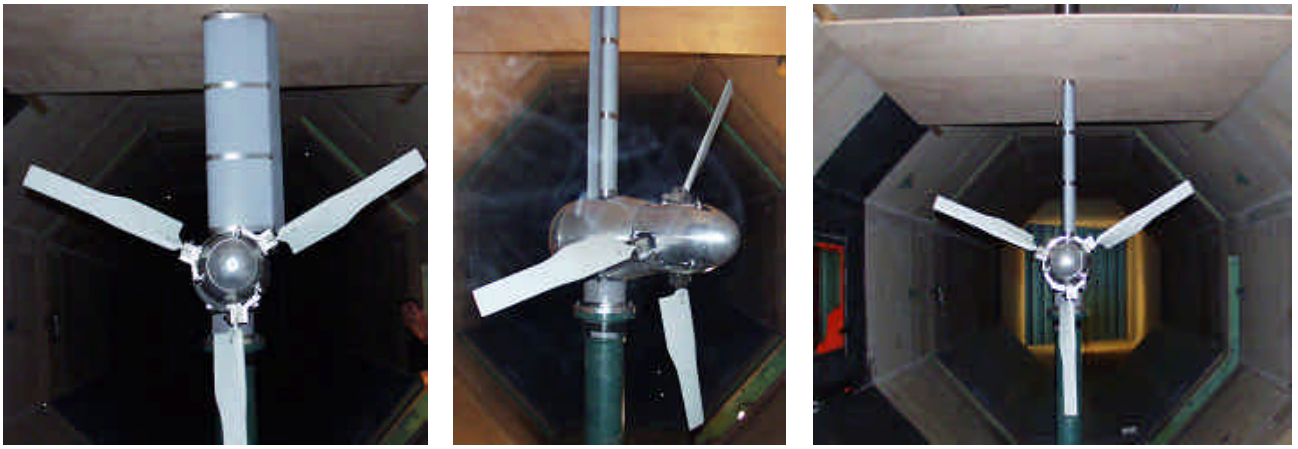

a b c

Fig. 2. Views of the tilt-rotor set-up

a) Hovering flight
b) Conversion flight
c) Cruise flight

The set-up also includes a fixed wing in the rotor wake as well as an end plane plate simulating the airframe (2m*2m*0.25m). The wing is maintained in the test section by a secondary rotating mast which is mounted on the upper part of the wind-tunnel test section. The wing has a span h=0.770m, a chord c=0.31m and is equipped with an OACV23 airfoil profile.

2.2 Experimental Technique

Overall aerodynamics performances on either the rotor blades or the fixed wing are performed by means of 6 components balances which provide global aerodynamic airloads, whereas local aerodynamics performances are measured using different complementary techniques. Indeed, for instance rotor tip paths can be determined using hot wire probes or 3C PIV, pressure coefficients distributions on the wing are measured by means of pressure sensors. The 3D velocity fields are measured using either Laser Doppler Velocimetry or 3C PIV. However, the flow between the rotor and a wing is shown to be described with more details and thus better analysed using the 3C PIV system which is more efficient in terms of measurement time and velocity field accuracy.

The stereoscopic PIV system includes two 200mJ Nd:Yag laser sources (QUANTEL Big Sky CFR200) operating at 532 nm, a frequency up to 15 Hz and two HISENSE PIV/PLIF cameras (1280x1024 pixels resolution) equipped with 35mm and 85mm Nikon AF Nikkor lens. The illuminating laser sheet is generated in a Z-plane normal to the uniform free stream velocity U_∞ as sketched in figure 3. Also shown in this figure are the illuminating laser sheet and the cameras positions around the tilt-rotor model.

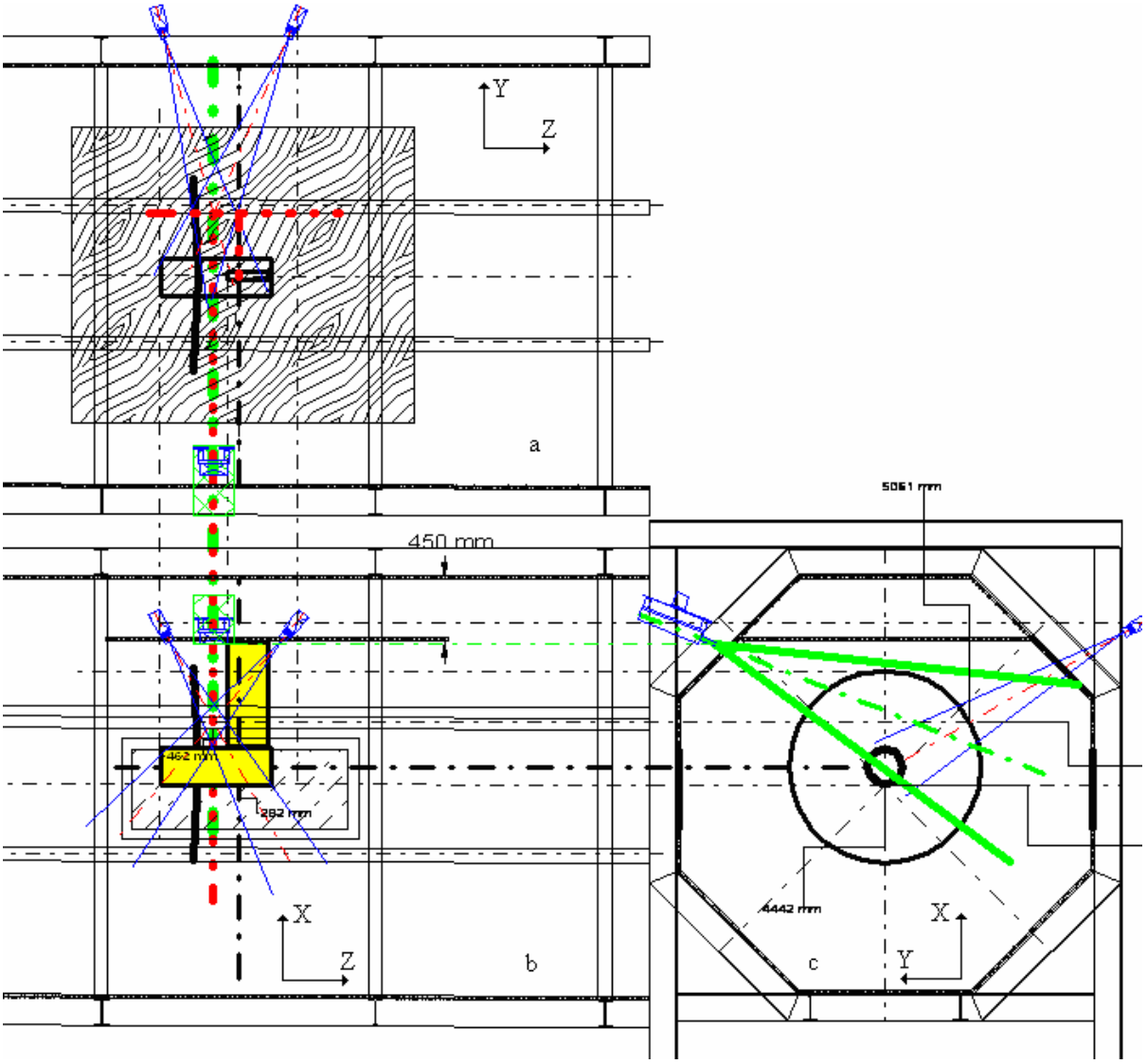

Fig.3. Schedule of PIV Set-up system

a) Top view of the wind-tunnel (Y, Z Plane)
b) Side view of the wind-tunnel (X, Z plane)
c) Transversal view of the wind-tunnel (X, Y Plane)

PIV measurements have been performed at different Z-planes distributed at different distance downstream the rotor. The wake regions between the rotor and the wing and above the fixed wing upper side have been more specifically investigated. To facilitate the viewing of the illuminated Z-planes the cameras are installed on a traversing system (3 degrees of freedom) located outside the wind-tunnel and close to the wall. The test section walls are equipped with ports holes to avoid refraction effects. Seeding of the flow was provided using particles generated by oil mixture having a nominal diameter of about 1µm.

2.3 Acquisition and Data Reduction Procedure

PIV images were phase-referenced to the blade azimuth position, to allow phase averaging of more than 100 images and thus increasing signal-to-noise ratio of the data. A specific processing of the data flow velocity sets was used to determine the PIV images at every 1 degree of azimuth through the 360° cycle of blade rotation. Acquisition and data analysis were done using the DANTEC

Flowmap PIV software. The data were then imported to a LabVIEW based post processing software for further data reduction and analysis.

The system operated in an adaptive correlation mode using pairs of images, which are compared from recordings by each camera over a 3µs delay in time. The adaptive correlation method calculates the velocity vectors within an interrogation area (IA). Before correlation, different filters were used to improve the particles images quality. A 16x16 pixels IA area was used, and the images were processed with 25% overlap yielding a raw vector field of 106x85 vectors. PIV measurements were performed using an observation field size of 320mm x 190mm and the light sheet thickness was of about 3 mm. The combination of the two-component vectors maps provides the 3C view of the flow where the magnitude of the out-of-plane velocity component is given by the coded colour scale. Figure 4 gives an example of a 3C instataneous velocity vectors field measurement with the corresponding out-of-plane vorticity component.

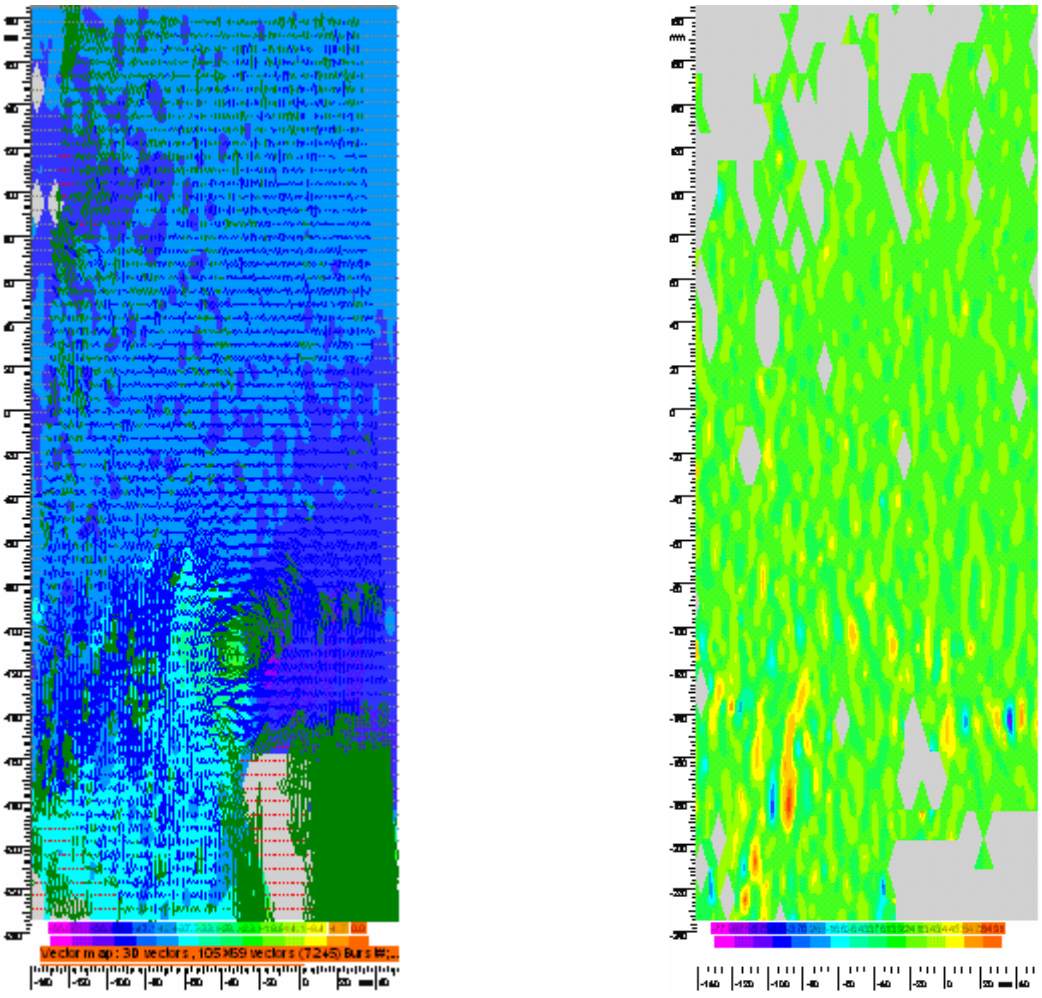

a b

Fig.4. 3C View of the instantaneous flow behind the blade for a 2deg azimuth of the blade

a) 3C Velocity vectors field

b) Out-of-plane vorticity component

However, such a data acquisition method still contains some erroneous vectors and thus a data phase averaging procedure has been applied on the velocity vectors maps in order to increase the reliability and accuracy of PIV measurements. At a given azimuth of the blade rotation, the statistical treatment is performed on at least 100 images (between 100 and 150) recorded by each

camera and the corresponding mean field vectors is the result of averaging the instantaneous records. An example of this phase averaging procedure over 100 instantaneous samples is given in figure 5 showing the mean velocity vectors and the associated out-of-plane vorticity component.

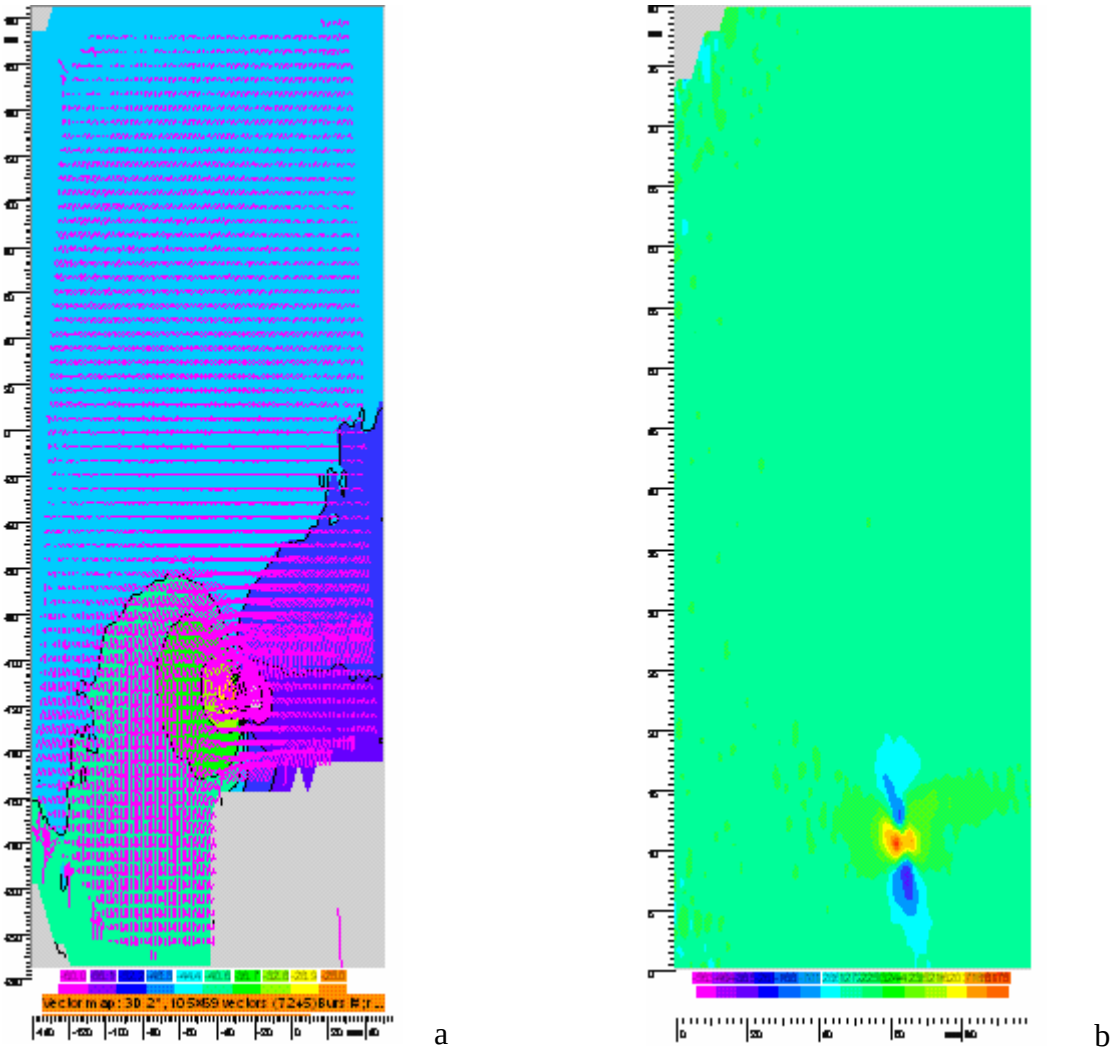

a b

Fig.5. 3C View of the mean flow behind the blade for a 2deg azimuth of the blade

a) 3C Velocity vectors field

b) Out-of-plane vorticity component

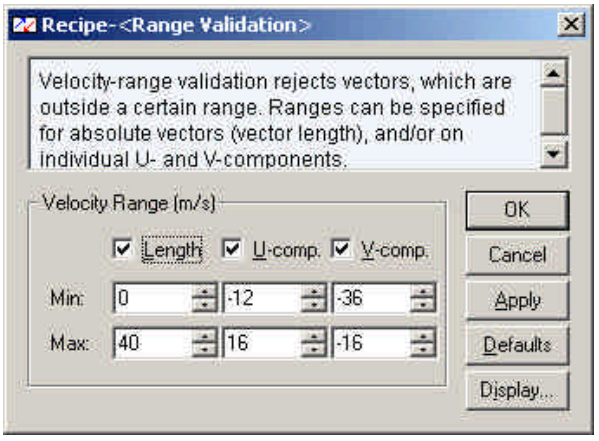

Fig.6. Range validation technique

A velocity range validation technique has been implemented in the procedure to reduce the number of erroneous vectors detected on each instantaneous vector fields as sketched in figure 6. On this table the minimum and maximum velocity values have been fixed as follows : $-12ms^{-1}<U<16ms^{-1}$; $-36ms^{-1}<V<-16ms^{-1}$. The velocity vector is then rejected when out of this range. An image dewarping function is also used to take into account the different angle distortions due to the cameras positions as regards to the free stream flow. The present results have generally shown that the averaging procedure applied on 100-150 images is providing reliable and repetitive data on both the velocity and the vorticity fields.

2.4 Vortex core localization technique

In order to automatically identify the tip vortex from the flow velocity vectors and to obtain an accurate localization of the vortex core center, a detection algorithm has been developed at LABM under Lab View software. From a phase averaged 3C velocity vectors field (as exemplified figure 5a), the method consists first to sum the instantaneous velocity along the X-coordinates for each line and to provide the X-location where the maximum of velocity value is reached. The same procedure is also applied along the Y-component. The maximum velocity value is thus obtained on each velocity component (U and V) and provides as a first estimate the XY-position of the vortex core center.

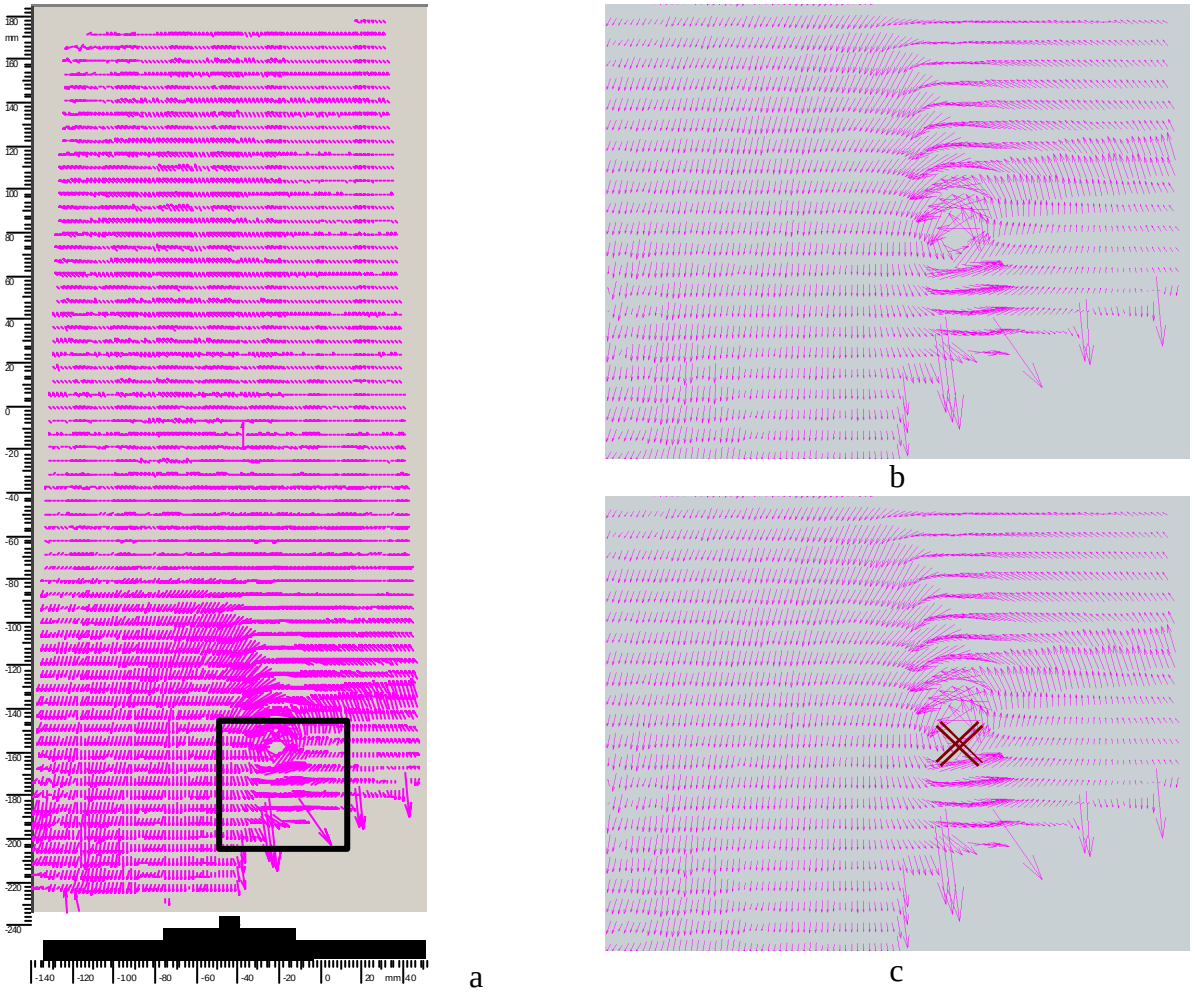

Fig.7. Schedule of LABM algorithm
a) 2D velocity vectors field *b) Zoom of 2D velocity vectors field*
c) Localization of the vortex core center

To increase the location accuracy, a zoom of the flow region around this first XY-position is then performed again as a second iteration. As shown in figure 7 the position of the vortex center (indicated by the cross) is automatically and accurately localized from the mean flow velocity vectors at the second iteration step. A number of 2-3 iterations are shown to be sufficient to obtain the accurate vortex core center position. This localization technique of the vortex core has been applied along different Z-planes in the rotor wake to determine the tip vortex paths associated to a given azimuth of the blade as discussed below in section 3.

2.5 Measurements Uncertainties

Accuracy of PIV system is generally shown to be dependent on many parameters but one of the main problems is to predict a good displacement of the same particle during a short time step. The displacement peak in the correlation plane is determined by means of a Gaussian function which should have a particle image diameter of about 2 pixels (whereas for higher values the random noise is significantly increased). The displacement peak has been indeed selected at a value of 2 pixels in the present adaptive correlation method.

Additionally the IA size also influences the accuracy of the particle displacement estimation. According to Raffel and Kompenhans (1998) the random noise increases from 0.01 pixels (for 64 pixels IA) to 0.1 pixels (for 16 pixels IA) as it is the case in the present experiments. However, the quantity of noise which could be accepted only depends on the physical component to be measured. For instance, the out-of-plane velocity component W (perpendicular to the laser light sheet), contains more noise than the two other components because W is deduced from a calculation on U and V. However, calculation performed on the averaged vectors field allows to decrease the influence of the random noise on the global error. Moreover, the software used to process the PIV images also introduces a random noise which remains less than 0.05 pixels over all the interrogation areas, excepted in the vortex core where there exist an important velocity gradient and a reduced seeding particles density. In this region the noise is increased to 0.1 pixels. Raffel and Kompenhans (1998) have estimated the in-plane displacement error at about 0.07 pixels and for the perpendicular-plane displacement at about 0.2 pixels. In the present experiments, the in-plane displacement is estimated at a value less than 4 pixels which corresponds to a total error of 2% on the two in-plane velocity component (U and V) and a total error of nearly 4% on the out-of-plane W velocity component.

3. Results and Discussion

PIV measurements are presented below in the cruise flight configuration and for the folowing set of parametric conditions on the rotor shaft angle (β=0deg), the blade rotational frequency (f=18.18Hz), the upstream velocity (U_8=46ms^{-1}), the advancing parameter ($\mu=U_8/2\pi fR$) and the collective pitch angle value (?=44deg). Figure 8 gives an example of the tip vortex imprint obtained in a fixed downstream plane (located at Z/R=0) and its associated 3C mean velocity field shed from the blade at 3 successive azimuth positions (ψ=1°, 2°, 5°). Plots of the mean velocity vectors clearly show the flow perturbation generated by the blade passage as well as the vortex development and propagation from the tip of the emitting blade which is shown in grey colour in Figure 8.

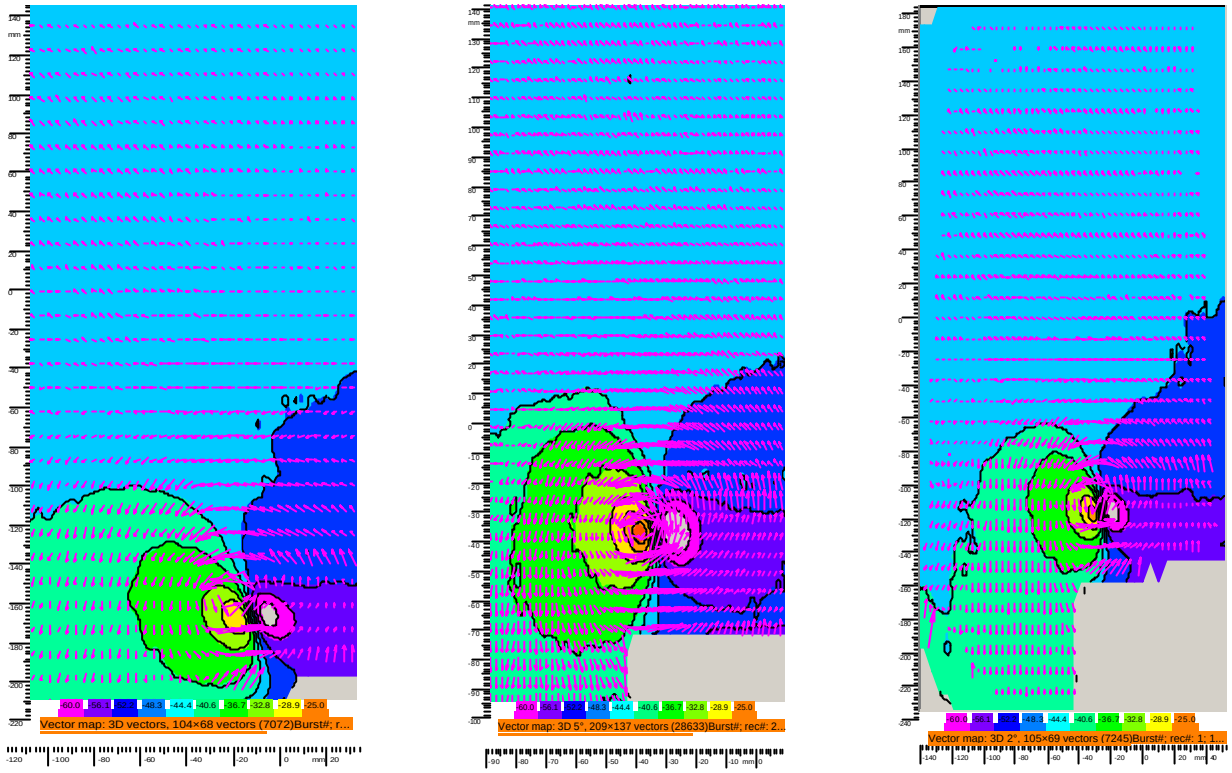

a b c

Fig.8. PIV measurements at plane Z/R=0 behind the blade in cruise flight conditions (b=0 deg, q=44 deg, U_8=46ms^{-1}, f=18.18Hz, m=0.575) and for 3 blade azimuth positions
a) y=1 deg
b) y=2 deg
c) y=5 deg

From such PIV measurements performed at different downstream Z-distances from the rotor and at different blade azimuth positions (ranging from ψ=0° to ψ=360°) the tip vortex paths have been reconstructed both in the wake region between the rotor and the wing and above the wing surface as shown in Figure 9. The results exhibit the wake geometry distortion due to the presence of the wing in the near wake.

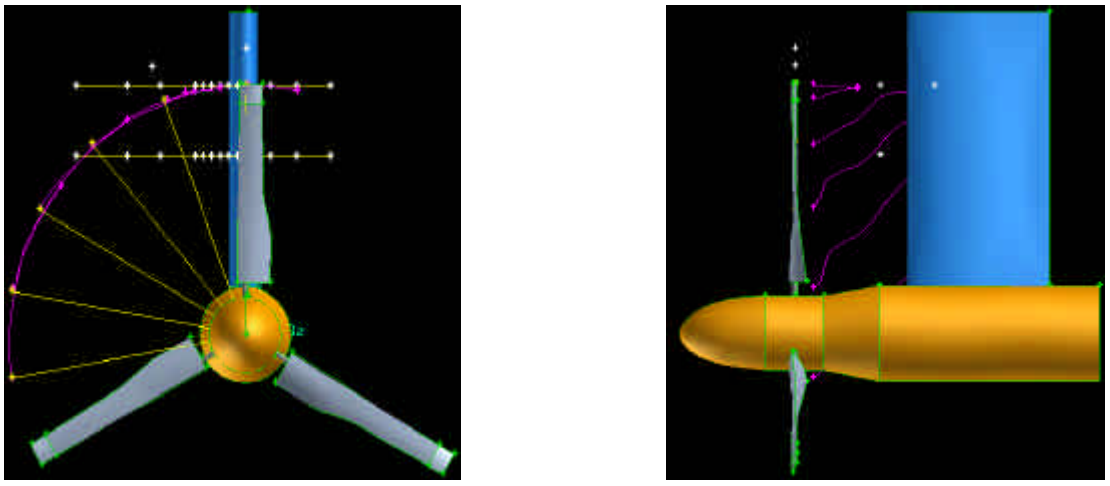

a b

Fig.9. Blade tip vortex paths in cruise flight: b=0 deg, q=44 deg, U_8=46ms^{-1}, f=18.18Hz, m=0.575
a) Front view b) Side view

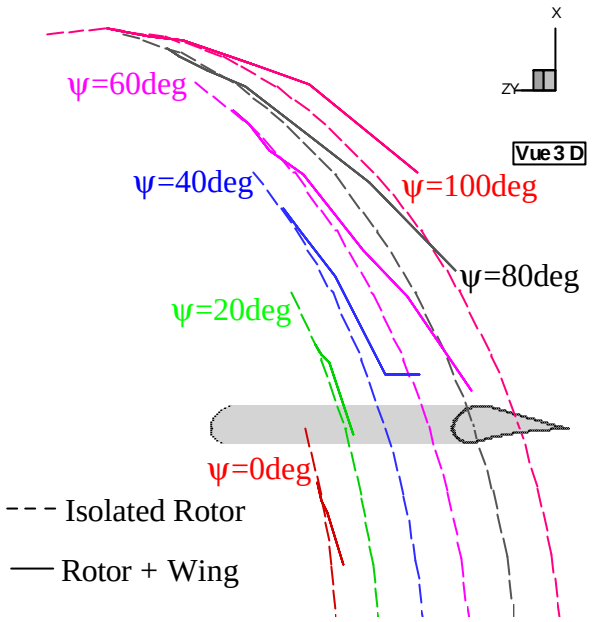

Fig.10. Tip paths in the isolated rotor wake (without wing, dotted lines) and in the cruise flight conditions (wing present, full lines): b=0 deg, q=44 deg, U_8=46ms^{-1}, f=18.18Hz, m=0.575

As an example the results in Figure 10 clearly show the change obtained in the tip vortex paths which are generated in the cruise flight configuration (when the wing is present) and are compared to the vortex trajectories corresponding to the isolated rotor (without the wing) for the same set of parametric flow conditions (f, U_8, μ, θ).

4. Conclusion and Perspectives

A stereoscopic PIV system has been used in the present study to investigate the vortical wake on a 1/7 tilt-rotor scale model operating in different flight configurations. The results show that the PIV method appears to be efficient for providing valuable data that characterize the vortex dynamics generated by the blade tips as a function of the blade azimuth. For a given flight configuration, the tip vortex paths can be determined over the whole blade rotation (360deg) and thus allow to accurately model the wake geometry distortion due to the wing and the corresponding flow conditions of interaction around the wing surface. In a near future, such PIV measurements will be also correlated with overall aerodynamic performance of the wing (Cl, Cd, Cm) in order to give more insight on the wing download/upload phenomenon that occurs in hovering and transition flight configurations on tilt-rotors.

References

Barla, Berton, Favier, Maresca (in press). "Boundary Layer Investigation on a tilt-rotor blade by means of an Embedded Laser Doppler Velocimetry", Journal of Aircraft.

Felker, Signor, Young, Betzina (1987). "Performance and Loads Data from a Hover Test of a 0.658-Scale V-22 Rotor and Wing", NASA TM 89419.

Felker and Light (1988). "Aerodynamics Interactions between a Rotor and Wing in Hover", Journal of the American Helicopter Society, Vol.33, No.2.

Johnson W. (1992-1997). "CAMRAD II, Comprehensive Analytical Model of Rotorcraft Aerodynamics and Dynamics", Johnson Aeronautics, Palo Alto.

Johnson W. (2000). "Calculations of TRAM Performance, Airloads and Structural Loads", Proceedings of the American Helicopter Society Specialists' Meeting Conference.

Johnson W. (2002). "Influence of Wake Models on Calculated Tilt-rotor Aerodynamics", Proceedings of the 58th Annual Forum of American Helicopter Society.

Matos, Reddy and Komerath (1999). "Rotor Wake/Fixed Wing Interactions with Flap Deflection", Proceedings of the 55th Annual Forum of American Helicopter Society.

McVeigh, Grauer, Paisley (1990). "Rotor/Airframe Interactions on Tilt-rotor Aircraft", Journal of the American Helicopter Society, Vol. 35, N°3.

Meakin (1995). "Unsteady Simulation of the flow about a V-22 Rotor and Wing in Hover", AIAA Paper 95-3463, Proceedings of the Atmospheric Flight Mechanics Conference.

Raffel, Kompenhans (1998). "Particle Image Velocimetry, A Practical Guide", Springer-Verlag.

Richard (2005). "Dynamique des tourbillons d'extrémité de pales de rotor en vol d'avancement", Thèse de Doctorat de l'Université de la Méditerranée.

Wood and Peryea (1986). "Reduction of Tilt-rotor Download", Proceedings of the 49th Annual Forum of American Helicopter Society.

Yamauchi, Burley, Mercker, Pengel, Janakiram (1999). "Flow Measurements of an Isolated Model Tilt-rotor", Proceedings of the 55th Annual Forum of American Helicopter Society.

Young, Lillie, McCluer, Yamauchi, Derby (2002). "Insights into Airframe Aerodynamics and Rotor-on-Wing Interactions from a 0.25 Scale Tilt-rotor Wind Tunnel Model", Proceedings of the American Helicopter Society Specialists' Meeting Conference.